Michigan State University

National Superconducting Cyclotron Laboratory

NUCLEAR FRAGMENTATION

Wolfgang Bauer

To be published in:
Proceedings of the Workshop on Fragmentation Phenomena,
Les Houches, France (1993)

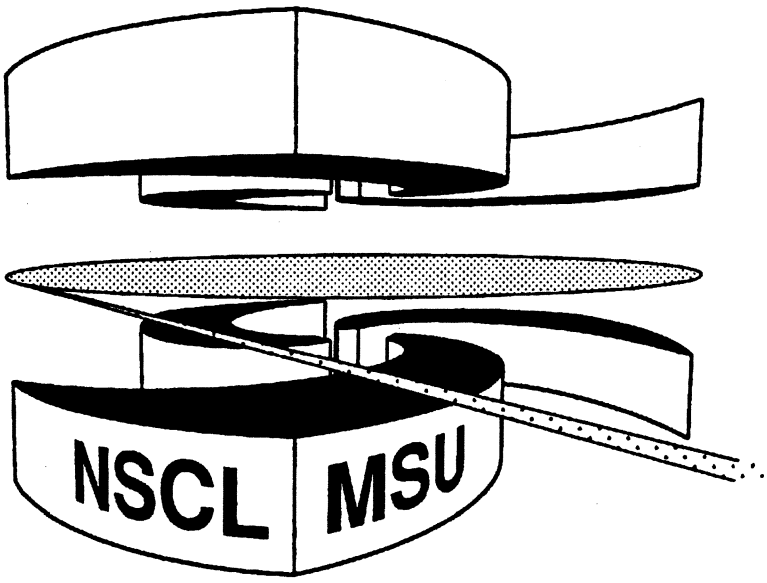

MSUCL-921 **February 1994**

NUCLEAR FRAGMENTATION

Wolfgang Bauer*

National Superconducting Cyclotron Laboratory *and*
Department of Physics and Astronomy
Michigan State University
East Lansing, MI 48824-1321, USA

Abstract. An introduction into a simple model of nuclear fragmentation, which is based on bond percolation, is given. Results are compared to experimental data for proton-induced reactions. In addition, dynamical aspects of nuclear fragmentation are discussed in the framework of a nuclear transport theory.

1. Introduction

The term 'nuclear fragmentation' refers to the decay of a nucleus into *several* smaller nuclei (fragments) and/or nucleons – as opposed to 'fission', where a big nucleus (such as, for example, uranium) splits into *two* smaller nuclei and several neutrons. To cause nuclear fragmentation a sizeable amount of energy (several MeV per nucleon) has to be imparted on the nucleus, whereas fission requires only the insertion of very small amounts of excitation energy and can in some cases (example: plutonium) even happen spontaneously. Fission derives its interest from its technological importance as the source of our nuclear energy. Nuclear fragmentation has at the present no direct technical applications in energy production, because in contrast to fission, one cannot generate a self-sustained chain reaction involving nuclear fragmentation events.

However, the investigation of nuclear fragmentation is very important, because it can offer us a glimpse into the nuclear equation of state due to the fact that the nucleus can undergo a phase transition in the process, as discussed below. Its importance beyond nuclear physics lies in the possibility to study extreme finite size effects on

* E-mail address: `bauer@nscl.nscl.msu.edu` (internet) or `bauer@msunscl` (bitnet)

the nature of phase transitions in systems with only several tens up to a few hundred constituents.

There are basically two distinct ways of causing nuclear fragmentation. In the first, one inserts excitation energy without sizeable compression into a nucleus. This can be done by bombarding the target nucleus with small hadronic projectiles such as protons, antiprotons, or pions, with small nuclei, or with electrons (virtual photons). The beam energy has to be on the order of a few GeV for this [1]. In the second mode of inducing nuclear fragmentation, one collides two nuclei of roughly equal mass, where compression to densities significantly above nuclear matter density is reached. Typical beam energies are on the order of 10-100 MeV per nucleon.

Due to the short duration ($\approx 10^{-22}$ to 10^{-20} seconds) of the fragmentation process and the microscopic dimension ($\approx 10^{-14}$ m) of the system, nuclear fragmentation cannot be directly observed. The only observables at our disposal are the masses and charges of the fragments as well as their asymptotic momenta when they reach the detectors. Thus we have to rely on modelling the fragmentation process and comparing the model predictions to experimental data.

Models can be divided into three categories: models assuming consecutive evaporation of fragments from the surface [2], models assuming more or less simultaneous break-up of the entire volume (multifragmentation) [3-19], and models in which the the decay proceeds via transiently reached non-compact topologies [20-23]. At low excitation energies, surface dominated emission is preferred. For nuclear fragmentation without sizeable compression and at high excitation energy, multifragmentation is dominating. The models describing this process often involve a phase transition, where the order and universality class of this transition should in principle be able to be determined in future experiments. A model of this kind, which has been particularly successful in reproducing experimental data, and which is conceptionally very simple, the percolation model of nuclear fragmentation [11-14,24-26], will be introduced in the following section. Its predictions will be compared to experimental data in section 3, and in section 4 finite size effects will be addressed. In section 5, the kinetic energy spectra of intermediate mass fragments are discussed. In section 6, I will briefly discuss the fragmentation process in the presence of sizeable compression in the initial stage leading to large radial outward flow, where a transport theoretical description of the reaction dynamics is required to understand the data.

Due to the inter-disciplinary character of these proceedings, I have attempted to present the essential concepts in a form, which can be understood by the non-specialist, leaving technical details to the cited publications in the specialized journals.

2. Percolation Model of Nuclear Fragmentation

In their ground state nuclei are made up of nucleons distributed with roughly constant density over the entire nuclear coordinate space volume. These nucleons interact via the short-range strong interaction with their nearest neighbors. In addition, the protons experience the long-range Coulomb interaction from all other protons in the nucleus. This is, to first order, the basis for the Bethe-Weizsäcker mass formula, which

approximately describes the binding energies of all nuclei.

In the standard model of nuclear bond percolation one represents the nucleons by sites on a simple cubic lattice in three dimensions and their nearest-neighbor interaction via bonds (compare Figure 1 for a two-dimensional illustration). The number of lattice sites is equal to the number of nucleons in the fragmenting system, and the occupied sites are arranged in a configuration which is approximately spherical (Figure 1 (a)). In the bulk, a nucleon shares 6 bonds with its neighbors. Since the nuclear matter binding energy is roughly 15.75 MeV, each bond represents an energy of 15.75/(6/2) MeV = 5.25 MeV. The missing bonds at the surface cause a reduction in the average binding energy just like in the Bethe-Weizsäcker formula. One can show that other lattice structure show very similar features, and that the conclusions reached are – to first order – independent of the specific lattice structure utilized.

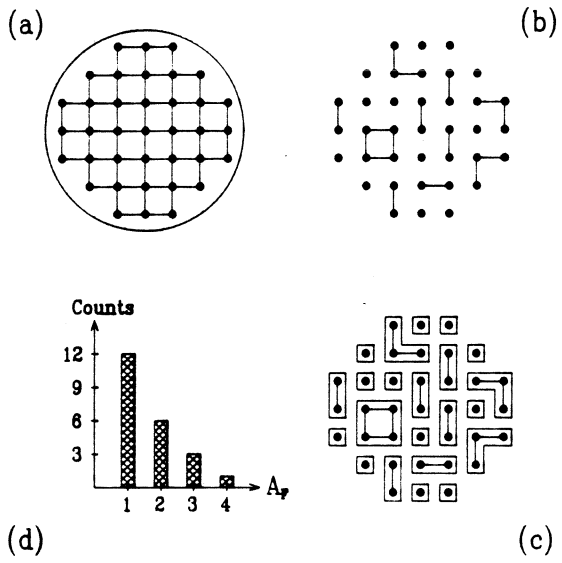

Figure 1. Illustration of percolation model

In high-energy ($E_{\mathrm{beam}} > 5$ GeV) proton induced reactions, the proton passes through the target nucleus on a basically straight line, interacting with the nucleons in its path. These participant nucleons are then ejected in forward direction, leaving behind an excited system of spectator nucleons [27]. We assume that the total excitation energy is uniformly distributed over the entire nuclear volume.[1] The addition

[1] One may also consider non-uniform distribution of excitation energy such as $p \propto r_{\perp}^{-\alpha}$, where $r_{\perp}$ is the radial distance to the path of the incident proton. This would be an indication of shock waves and has proven to be successful in percolation description of rock fragmentation (see the contribution of R. Englman to this volume). However, we have obtained best results with the uniform distribution, indicating equilibration.

of excitation energy causes bonds to be randomly broken with a breaking probability p. (Figure 1 (b)). Sites still connected to each other via the remaining bonds are identified as clusters (Figure 1 (c)), where the fragments mass is given by the number of sites in the cluster. In this way one obtains a fragment mass distribution (Figure 1 (d)).

Before one can compare the predictions of the model to experimental fragment production data, one has to take care of an additional complication: In proton-induced reactions the amount of deposited energy depends on the impact parameter, b. We assume that the total energy deposited is proportional to the number of nucleon-nucleon collisions experienced by the projectile on its (straight-line) path through the target. This leads to an impact parameter dependence [13]

$$p(b) = p_0 \frac{\int dz\, \rho(x=b, y=0, z)}{\int dz\, \rho(0,0,z)} \ , \tag{1}$$

where $\rho(x,y,z)$ is the matter density of the target nucleus, and $p_0 = p(b=0)$.

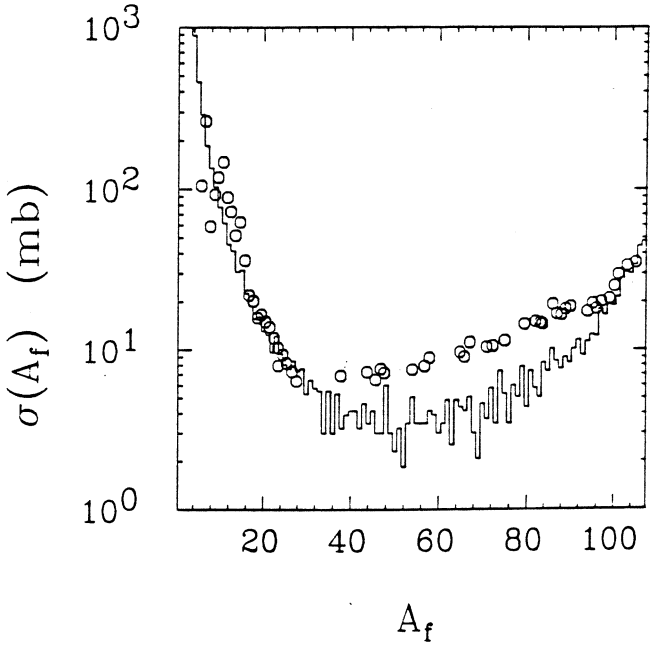

Figure 2. Fragment production cross section

3. Comparison to Data

One can compare the predictions of the percolation model to experimental data by computing the total fragment production cross section

$$\sigma(A_f) = 2\pi \int_0^{b_{max}} b\, db\, \frac{N(A_f, b)}{N_{run}(b)} \ , \tag{2}$$

where $N(A_f, b)$ is the total number of fragments of mass A_f obtained in N_{run} events generated with breaking probability $p(b)$ at impact parameter b.

Figure 2 shows a representative comparison of the nuclear percolation model (histogram) to experimental data (circles) [3,4,28] for the system p+Ag at a proton energy of 300 GeV (only a fraction of this energy is actually deposited into the target). First, it is clear that the overall normalization of the fragment production cross sections are reproduced amazingly well considering the exceedingly simple model. One can see that the characteristic U-shape of the experimental mass yield curve is nicely reproduced by the calculations. This is a consequence of the contributions of different impact parameters with different excitation energies. Less apparent in this display is the fact that the cross section for the production of small to intermediate mass fragments approximately follows a power law

$$\sigma(A_f) \propto A_f^{-\lambda} \ . \tag{3}$$

It is well known [29,14] that scaling theories of phase transitions predict a fragment number (which is proportional to the cross section) distribution

$$N(A_f, p) = A_f^{-\tau} \, f(A_f^{\sigma} \cdot (p - p_c)) \tag{4}$$

near the critical point, where the function f has to fulfill the condition $f(0) = 1$, and τ and σ are the critical exponents and have the values 2.2 and 0.45, respectively, for 3d percolation. p_c is the critical value of the breaking probability with a numerical value of 0.75 for our system.

It is then obvious that at $p = p_c$ the fragment size distribution follows a power law, and the fact that one extracted a power law from the experimentally measured fragment cross sections (with $\lambda \approx 2.6$ in Equation (3)) triggered a flood of speculations on the observation of a phase transition in nuclear fragmentation [4,8-10,14].

However, we showed [11] that the occurrence of a power law fragment distribution is not a sufficient condition for a critical point. Rather it is always possible for finite systems in the vicinity of the critical point to fit the fragment spectra to a power law with an effective exponent λ, and $\min\{\lambda\} = \tau$ at the critical point. The result of our studies is that one should in principle be able to approach the critical point of the nuclear matter phase diagram in nuclear fragmentation studies, but one has to take care to fix the excitation energy deposited to a single value. This can, for example, be done in an event-by-event analysis of fragmentation data.[2] Experiments of this kind are in progress or in the planning stages. The GSI Aladin group, for example has studied the excitation function for multifragmentation [25,30,31] events in E/A = 600 MeV Au-induced reactions on light targets, and their preliminary analysis shows that the percolation model of nuclear fragmentation is best able to describe the data gathered by them [25]. For near symmetric systems, the MSU-4π group has investigated the beam energy dependence of the fragment mass yield and finds again very good agreement with the percolation model [32].

[2] X. Campi has suggested this approach – see his contribution to this volume.

4. Finite Size Effects

One of the reason that nuclear fragmentation is of importance beyond nuclear physics is, as mentioned above, the fact that it enables us to study extreme finite size effects in phase transitions. Within the percolation model, for example, one may investigate the fractional shift in the critical value of the breaking probability, for which we have numerically found [12] the power-law dependance

$$\epsilon(n) = \frac{p_c(n) - p_c(\infty)}{p_c(\infty)} \approx 0.2\, n^{-1/\nu} \ , \tag{5}$$

where $n \times n \times n$ is the size of the lattice, and ν is a critical exponent with value 0.9.

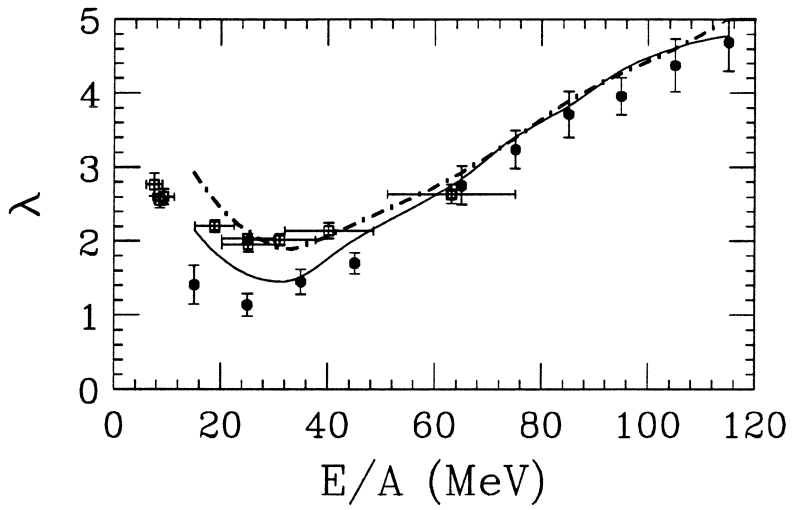

Figure 3. Apparent exponent τ versus beam energy

We also find [32] that the critical exponent τ is not independent of n, and that it can have values significantly smaller than its bulk matter value of 2.2. Figure 3 shows the extracted values of τ from the fragment charge distributions of fragments obtained from heavy ion fragmentation as a function of the deposited excitation energy. The solid plot symbols are experimental data for the reactions E/A = 600 MeV Au+C, Al, Cu (with excitation energy converted to an equivalent beam energy for symmetric systems), and the open plot symbols are for the reaction Ar+Sc. The solid and dashed lines are the results of percolation calculations with N=68 and N=150 nucleons, respectively.

Another important finite size effect is that the equivalent of the infinite percolation cluster becomes finite in finite systems. This is of importance in, for example, the moment analysis of fragment size distributions which is used to determine the location of the critical point and the value of the critical exponents in event-by-event analysis. We find [13] that one can most effectively eliminate the effect of the percolation cluster

by introducing a cutoff mass, $A_{\rm cut}$, in the defining equation for moments $M_i(p)$

$$M_i(p) = \sum_{A_{\rm f}=1}^{A_{\rm cut}} (A_{\rm f})^i \, N(A_{\rm f}, p) \; . \tag{6}$$

From numerical studies we find that $A_{\rm cut} \approx (A_t + A_p)/3$ effectively eliminates the contributions of the percolation cluster. The standard prescription [14] to simply omit the largest cluster found in the event from the analysis leads to wrong results in the presence of fission events, where the one fission product left in the sample will generate very large value of the moments.

5. Kinetic Energy Spectra of Intermediate Mass Fragments

The experimentally observed kinetic energy spectra of intermediate mass fragments are conventionally parametrized by a Maxwell-Boltzmann distribution in the rest frame of the emitting system [33,34,4]

$$\frac{d^2\sigma(A_{\rm f})}{dE^* d\Omega^*} = \frac{\sigma_0}{2\,(\pi T)^{3/2}} \sqrt{E^*} \exp(-E^*/T) \; , \tag{7}$$

where E^* is the available kinetic energy

$$E^* = \frac{A_{\rm total}}{A_{\rm total} - A_{\rm f}} \, E' - \kappa \, B \tag{8}$$

and B is the Coulomb barrier

$$B = \frac{e^2 \, (Z_{\rm total} - Z_{\rm f}) \, Z_{\rm f}}{r_0 \, (A_{\rm f}^{1/3} + (A_{\rm total} - A_{\rm f})^{1/3})} \; . \tag{9}$$

This parametrization assumes a functional shape motivated by a two-body breakup. However, the measured Coulomb barriers are much lower than expected from this geometry [4]. Hence the fit constant κ ($\kappa < 1$) has been introduced. The 'temperature', T, is another fit parameter and has in general a value of above 10 MeV.

In the following we will show that this minimum apparent temperature can be understood as a consequence of the Fermi-Dirac statistics of the nucleons, and that the reduction in the Coulomb barrier can be understood as a consequence of a simultaneous multifragmentation of a system with mass $A_{\rm total}$ and charge $Z_{\rm total}$.

5.1. Apparent Fragment Temperature

Let us assume that a nucleus is equilibrated at some excitation energy. The nucleons inside the nucleus are then distributed according to a Fermi-Dirac distribution with a temperature, which we will call $T_{\rm in}$. We assign each nucleon a momentum

$$\vec{p_i} = (\xi_1, \xi_2, \xi_3) \, \hbar \, k_F(\rho(\vec{r_i}), T_{\rm in}) \; , \tag{10}$$

where ξ_1, ξ_2, and ξ_3 are random numbers with $\sum_j (\xi_j)^2 \leq 1$.

Following Feshbach and Huang [35] and Goldhaber [36], the individual momenta of the fragments add up to the total momentum $\vec{P}_\mathrm{f}$ of the fragment

$$\vec{P}_\mathrm{f} = \sum_{i=1}^{A_\mathrm{f}} \vec{p}_i \ . \tag{11}$$

The resulting fragment kinetic energy distribution follows then approximately a Maxwell-Boltzmann distribution function with apparent temperature T_out. This result can be either approximately obtained by integrating over the nucleon momentum distribution functions with the constraint $\delta(\vec{P}_\mathrm{f} - \sum_i \vec{p}_i)$, or it can be obtained numerically by a Monte Carlo integration method. We chose the latter and present the result in Figure 4, represented by the plot symbols with the statistical error bars from the integration procedure.

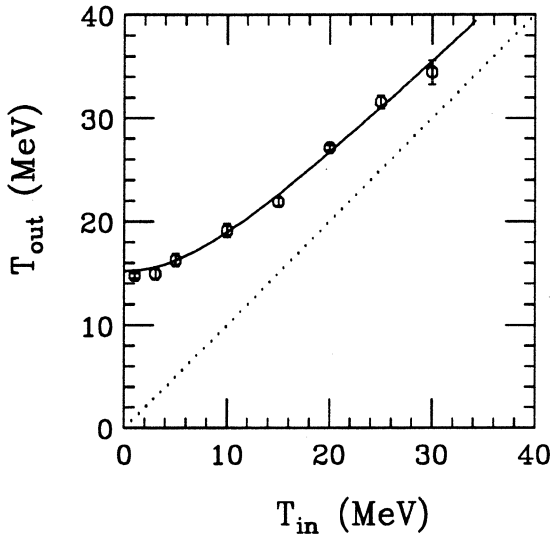

Figure 4. Observed kinetic temperature vs. internal temperature

The dotted diagonal line in Figure 4 represents $T_\mathrm{in} = T_\mathrm{out}$. It is approached in the limit of large temperatures, as expected. The solid line corresponds to

$$T_\mathrm{out} = \tfrac{2}{3} \langle E_\mathrm{kin}(T_\mathrm{in}) \rangle \ , \tag{12}$$

where $\langle E_\mathrm{kin}(T_\mathrm{in}) \rangle$ is the mean kinetic energy of nucleons distributed according to a Fermi-Dirac distribution at temperature T_in. This is again the classical limit. This result and that the fragment distribution function is of Maxwell-Boltzmann shape are consequences of the integration over the distribution functions of the individual nucleons in the fragment. However, the fact that the mean kinetic energy of the nucleons does not go to 0 as $T_\mathrm{in} \rightarrow 0$ is a consequence of the Fermion character of the nucleons inside the fragments, and so is the minimum apparent temperature of intermediate mass fragments.

The minimum value of the apparent fragment temperature for fragments emitted from an infinitely big system is then $T_{\mathrm{out},\infty} = \frac{2}{5} E_F$, where E_F is the Fermi energy. This value is somewhat lowered in finite systems due to a reduction of the average Fermi energy as, for example, described by the local Thomas-Fermi approximation, and by a factor $A_{\mathrm{total}}/(A_{\mathrm{total}} - A_{\mathrm{f}})$ due to the recoil correction of Equation (8), a consequence of the 0 total momentum of the emitting system in its rest frame before the emission of the fragment.

It should be pointed out that this effect of an 'output temperature' different from the 'input temperature' explains the apparent contradiction between 'temperatures' extracted from kinetic energy spectra and 'temperatures' extracted via other means such as level population ratios [37-40].

5.2. Reduced Coulomb Barriers

We now proceed to calculate kinetic energy distributions of intermediate mass fragments to be compared with experiment. To do this, we generate fragmentation events in our percolation model and initialize the fragment momenta as described in the last subsection. The fragments then have to be propagated under the influence of the many-body Coulomb expansion. To do this, we also have to provide initial conditions for the coordinate space locations of the fragments as well. The locations of the fragments in coordinate space can be calculated from their locations on the lattice using

$$L = (\rho_{\mathrm{f}})^{-1/3} \ , \tag{13}$$

where L is the lattice spacing and ρ_{f} is the so-called freeze-out density, the density below which the strong interaction becomes negligible. The location of the peak in the fragment energy spectra is sensitive to the value chosen for ρ_{f}, and we obtain best agreement with the data for $\rho_{\mathrm{f}} = 0.36$ fm^{-3}.

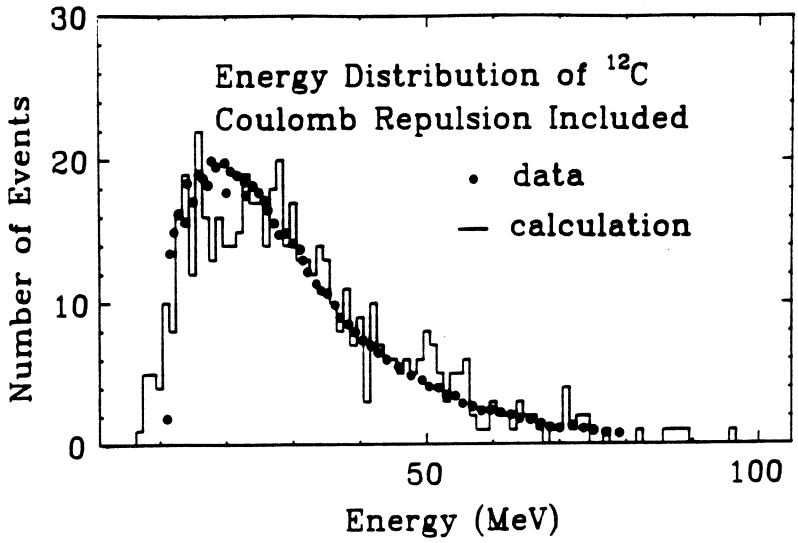

Figure 5. Fragment energy spectra

In Figure 5 we compare the the result of this calculation (histogram) with the data (circles, [4]) for the kinetic energy distribution of ^{12}C fragments produced in interaction of 80-300 GeV protons with Xe. One can see the good agreement in the fall-off constant as well as the maximum of the distribution, which is located at 28 MeV. For comparison, the Coulomb barrier as calculated with Equation (9) for the emission of ^{12}C from Xe is $\approx$ 48 MeV.

The 'kinetic temperature' of the carbon fragments from the xenon fragmentation is in our picture caused by the random coalescence of nucleons with their corresponding Fermi-momenta inside the fragments, and the large reduction of the Coulomb barrier is due to the simultaneous multifragmentation of the entire nucleus in a volume-dominated emission process.

6. Fragmentation of Non-Compact Nuclear Shapes

Up to now, we have only discussed the fragmentation of spectator matter in proton-induced reactions at high energies. As mentioned before, it is also possible to consider central reactions of targets and projectiles of roughly equal mass at much lower beam energies (below E/A = 100 MeV). Here the participant matter is excited to energies necessary for the occurrence of multifragmentation. This approach, however, may lead to dynamical, non-statistical contributions to the fragmentation process.

In a recent paper [21], we have used microscopic nuclear transport calculations [53-55] to show that in central or near-central collisions of nuclei of about equal mass at beam energies of E/A $\approx$ 50-60 MeV unstable hollow configurations (bubbles and/or rings) may be formed transiently. A result of this calculation is shown in figure 6, where we display the nucleon density in the reaction plane (x-z plane at y=0) for the central reaction ^{93}Nb + ^{93}Nb at E/A = 60 MeV. After t = 160 fm/c, one can clearly see two bumps, which indicate the formation of a doughnut-shaped object perpendicular to the beam axis.[3]

Even without detailed calculations it is possible to understand qualitatively the reasons for the formation of hollow structures in this class of nuclear reactions. Let us start with a compressed hot nuclear system. As it expands its outer surface forms a radially outgoing density wave. This density wave is fed by an inward traveling rarefaction wave. Assuming for simplicity radial symmetry, we can then write the mass continuity equation as

$$r_{\rm out}^{\alpha}\,\rho(r_{\rm out})\,v_{\rm out} = r_{\rm in}^{\alpha}\,[\rho_c - \rho(r_{\rm in})]\,v_{\rm in}\ , \qquad (14)$$

where α has a value between 1 and 2. Here $r_{\rm in}, r_{\rm out}$ and $v_{\rm in}, v_{\rm out}$ are the locations and velocities of the the surfaces of the inward and outward propagating wave fronts, respectively. As the rarefaction wave moves in toward the center, the right hand side of equation (14) decreases. As long as there is a well defined surface with finite density

[3] The intersection of a torus and a plane through the torus' symmetry axis results in two circles, corresponding to the two density bumps shown in the figure.

Nb + Nb, E/A = 60 MeV, b = 0 fm

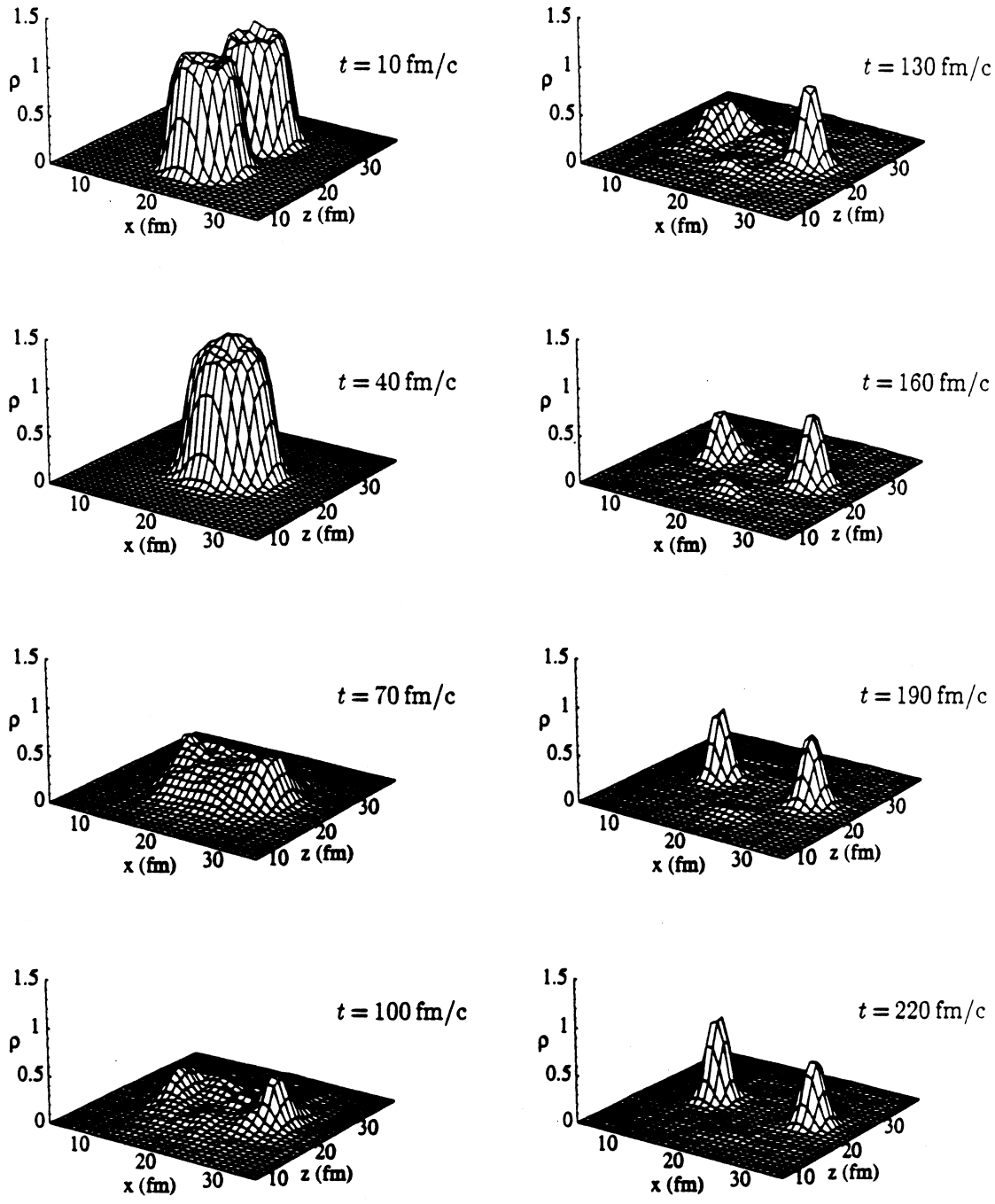

Figure 6. Occurrence of non-compact configurations

$\rho(r_{out})$, the outflow velocity v_{out} must decrease and eventually approach 0.[4] Matter close to the center of mass is still streaming outward when the rarefaction reaches the center, and the interior or the nuclear system is depleted of baryon density (t = 100-130 fm/c). This gives rise to the occurrence of bubble and doughnut like shapes of the density profile.

Other groups have observed similar results in their simulations of heavy ion reactions [20,22,41-43] or in studies of hot static nuclei [44-46]. The Coulomb interaction seems to have an essential role in the formation and the stabilization of these objects [23]. The transiently formed hollow configurations are not absolutely stable, however, because of the onset of dynamic instabilities caused by the compressibility

$$\mathcal{C} = v_s^2 = \left.\frac{\partial P}{\partial \rho}\right|_S \tag{15}$$

reaching negative values [21], which results in the exponential growth [47] of small fluctuations [48] and a breakup of the system.[5]

There are observable consequences of the formation of these hollow configurations. First, the energy spectra of intermediate mass fragments (IMFs) should be different, with a maximum a lower energies than obtained from the reactions discussed in section 5. One should also expect an observable difference in IMF-IMF correlation functions. Work on this is currently in progress [49]. And a third consequence is a different mass distribution of intermediate mass fragments.

In the context of the percolation model introduced above, we have recently investigated the shape of the fragment mass yield curve for non-compact objects [50]. We find that even for systems of large mass, in which the finite size effects discussed in section 4 play only a very small role, the occurrence of non-compact breakup configurations has large observable consequences. From our calculations we conclude that the breakup of bubbles and doughnuts still leads to fragment mass distributions, which can be fit with equation (3), but with an exponent λ, which can be significantly lower than for compact systems of the same mass number.

In figure 7, we show one of the results of our study [50]. Displayed is the effective exponent λ of equation (3) as a function of the breaking probability, p, and the inner radius, R_b, of the bubble for a bubble of 250 nucleons. One can clearly see that λ reaches values as low as 1.7, which should be compared to $\min[\lambda] = 2.2$ for the same system in a compact breakup geometry. This lower value of lambda also is able to explain the observation that there is a much larger number of IMFs per charged particle in near symmetric projectile/target mass systems than in asymmetric ones [51,52].

---

[4] In case that the radial kinetic energy is large compared to the nuclear binding energy, the out-flowing matter vaporizes and equation (14) is fulfilled with $\rho(r_{out}) \rightarrow 0$.

[5] However, the transport calculations are based on a time-evolution of the one-body density and are thus not able to reproduce the final fragment distribution after break-up. For this, molecular dynamics simulations [16-19] are more suitable.

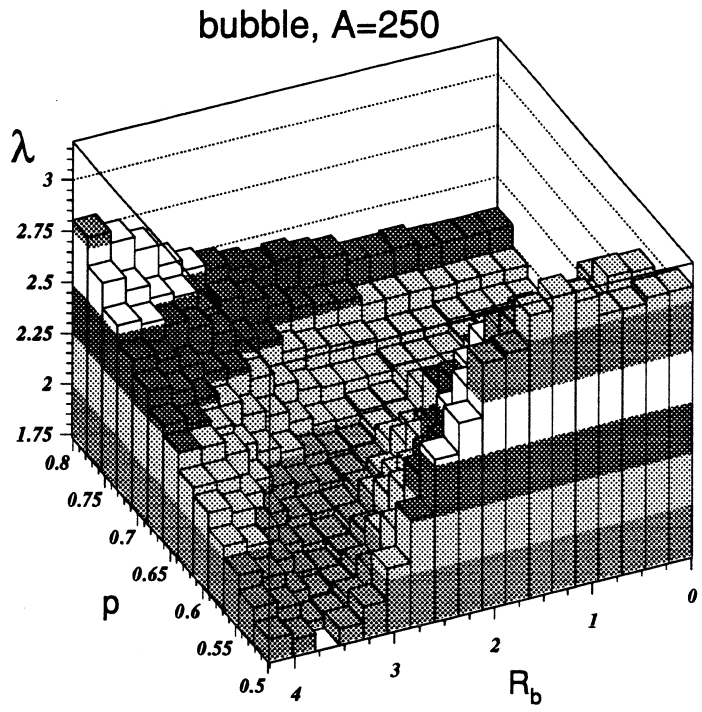

Figure 7. Dependence of effective exponent λ on p and R_b

7. Summary

The investigation of nuclear fragmentation has reached a *quantitative* stage. With the present 4π fragment detection arrays one is now able to study fragmenting nuclear systems on an event-by event basis. In these experiments it is possible to carefully select nuclear systems prepared at a fixed initial excitation energy.

We can now perform detailed comparisons to dynamical and statistical theories of nuclear fragmentation. However, as all theories have some limited realm of validity, we cannot expect one theory to fit every phenomenon encountered.

In fragmentation events without significant transient compression of nuclear matter, models based on the assumption of the establishment of some sort of energy-equilibration seem to work well to describe the observables presently under consideration. Among these are theories such as the percolation model introduced above which contain phase transitions of first or second order. This indicates that it may be possible to observe critical behavior due to a second order phase transition of nuclear matter in multifragmentation events.

At the present stage we cannot uniquely determine *one* right class of theories of nuclear fragmentation - there are many candidates which can fit experimental observables, provided the fit parameters in the theories can be adjusted. In addition, the experimental determination of the critical exponents of the nuclear fragmentation phase transition is complicated by finite size effects discussed in section 4 and by dynamical effect such as the one mentioned in section 6.

However, it is clear that the experimental and theoretical study of nuclear fragmentation will enjoy a fruitful mutual interaction for several years to come, and important results for the nuclear equation of state and many-body theory of small systems can be expected.

The author wishes to acknowledge many fruitful collaborations with G.F. Bertsch, D.R. Dean, C.K. Gelbke, T. Li, U. Mosel, L. Phair, U. Post, H. Schulz, and G.D. Westfall, which have led to some of the results presented above. Partial support for this research was provided by the US National Science Foundation under grants number PHY-8906116 and PHY-9017077 as well as a National Science Foundation Presidential Faculty Fellow award.

References

[1] J. Hüfner, *Phys. Rep.* **125** 131 1985.
[2] W.A. Friedman and W.G. Lynch, *Phys. Rev. C* **28** 16 1983.
[3] R.W. Minich *et al* , *Phys. Lett. B* **118** 458 1982.
[4] A.S. Hirsch *et al* , *Phys. Rev. C* **29** 508 1984.
[5] J.P. Bondorf, *Nucl. Phys. A* **387** 25c 1982.
[6] J. Randrup and S.E. Koonin, *Nucl. Phys. A* **356** 223 1981.
[7] D.H.E. Gross *et al* , *Z. Phys. A* **309** 41 1982.
[8] M.W. Curtin *et al* , *Phys. Lett. B* **123** 289 1983.
[9] L.P. Csernai and J.I. Kapusta, *Phys. Rep.* **131** 223 1986.
[10] P.J. Siemens, *Nature (London)* **305** 410 1983.
[11] W. Bauer *et al* , *Phys. Lett. B* **150** 53 1985.
[12] W. Bauer *et al* , *Nucl. Phys. A* **452** 699 1986.
[13] W. Bauer, *Phys. Rev. C* **38** 1297 1988.
[14] X. Campi, *Phys. Lett. B* **208** 351 1988.
[15] C.K. Gelbke and D.H. Boal, *Prog. Part. Nucl. Phys.* **19** 33 1987.
[16] J. Aichelin and H. Stöcker, *Phys. Lett. B* **176** 14 1986.
[17] J. Aichelin, *Phys. Rep.* **202** 233 1991.
[18] D.H. Boal and J.N. Glosli, *Phys. Rev. C* **38** 1870 1988.
[19] D.H. Boal and J.N. Glosli, *Phys. Rev. C* **42** R502 1988.
[20] L. Moretto *et al* , *Phys. Rev. Lett.* **69** 1884 1992.
[21] W. Bauer *et al* , *Phys. Rev. Lett.* **69** 1888 1992.
[22] D.H.E. Gross *et al* , *Ann. Physik* **1** 467 1992.
[23] B. Borderie *et al* , *Phys. Lett. B* **302** 15 1993.
[24] J. Desbois, *Nucl. Phys. A* **466** 724 1987.
[25] U. Lynen, *Nucl. Phys. A* **545** 329c 1992.
[26] X. Campi and H. Krivine, *Nucl. Phys. A* **545** 161c 1992.
[27] R. Serber, *Phys. Rev.* **72** 1114 1947.
[28] A. Bujak *et al* , *Phys. Rev. C* **32** 620 1985.
[29] D. Stauffer, *Phys. Rep.* **54** 1 1979.
[30] A. Hubele *et al* , *Z. Phys. A* **340** 263 1991.
[31] C.A. Ogilvie *et al* , *Phys. Rev. Lett.* **67** 1214 1991.

[32] T. Li *et al* , *Phys. Rev. Lett.* **70** 1924 1993.
[33] G.D. Westfall *et al* , *Phys. Rev. Lett.* **37** 1202 1976.
[34] G.D. Westfall *et al* , *Phys. Rev. C* **17** 1368 1978.
[35] H. Feshbach and K. Huang, *Phys. Lett. B* **47** 300 1973.
[36] A.S. Goldhaber, *Phys. Lett. B* **53** 306 1974.
[37] J. Pochodzalla *et al* , *Phys. Rev. C* **35** 1695 1987.
[38] Z. Chen *et al* , *Nucl. Phys. A* **473** 564 1987.
[39] Z. Chen *et al* , *Phys. Rev. C* **36** 2297 1987.
[40] H.W. Barz *et al* , *Phys. Lett. B* **217** 397 1989.
[41] P. Schuck *et al* , *Prog. Part. Nucl. Phys.* **22** 181 1989.
[42] L. Vinet *et al* , *Nucl. Phys. A* **468** 312 1987.
[43] J. Nemeth *et al* , *Z. Phys. A* **323** 419 1987.
[44] C.Y. Wong, *Ann. Phys. (New York)* **77** 279 1973.
[45] A. Dhar and S. Das Gupta, *Phys. Rev. C* **30** 1545 1984.
[46] C.Y. Wong, *Phys. Rev. Lett.* **55** 1973 1985.
[47] C.J. Pethick and Ravenhall, *Nucl. Phys. A* **471** 19c 1987.
[48] W. Bauer *et al* , *Phys. Rev. Lett.* **58** 863 1987.
[49] T. Glasmacher *et al* , *Preprint MSUCL-893* 1993.
[50] L. Phair *et al* , *submitted to Phys. Lett. B* 1993.
[51] L. Phair *et al* , *Phys. Lett. B* **285** 10 1992.
[52] D.R. Bowman *et al* , *Phys. Rev. C* **46** 1834 1992.
[53] W. Bauer *et al* , *Phys. Rev. C* **34** 2127 1986.
[54] W. Bauer, *Phys. Rev. Lett.* **61** 2534 1988.
[55] W. Bauer *et al* , *Annu. Rev. Nucl. Part. Sci.* **42** 77 1992.